Article

Triple isotope fractionation exponents of elements measured by MC-ICP-MS - an example of Mg

Michael Tatzel, Jochen Vogl, Martin Rosner, Michael Henehan, and Thomas Tütken

Just Accepted

Triple isotope fractionation exponents of elements measured by MC-ICP-MS - an example of Mg

Michael Tatzel[1][*][†], Jochen Vogl[1], Martin Rosner[2], Michael J. Henehan[3], Thomas Tütken[4]

[1] Bundesanstalt für Materialforschung und -prüfung (BAM), Richard-Willstätter Str. 11, 12489 Berlin, Germany

[2] IsoAnalysis UG, 10829 Berlin, Germany

[3] GFZ German Research Centre for Geosciences, 14473 Potsdam, Germany

[4] Institute of Geosciences, Applied and Analytical Palaeontology, University of Mainz, 55128 Mainz, Germany

ABSTRACT: In most chemical reactions, stable isotopes are fractionated in a mass-dependent manner, yielding correlated isotope ratios in elements with three or more stable isotopes. The proportionality between isotope ratios is set by the triple isotope fractionation exponent, θ, that can be determined precisely for *e.g.* sulfur and oxygen by IRMS, but not for metal(loid) elements due to the lower precision of MC-ICP-MS analysis and smaller isotopic variations. Here, using Mg as a test case, we compute a complete metrologically-robust uncertainty budget for apparent θ-values, and with reference to this, present a new measurement approach that reduces uncertainty on θ-values by 30 %. This approach, namely direct educt-product bracketing (sample-sample bracketing), allows apparent θ-values of metal(loid) isotopes to be determined precisely enough to distinguish slopes in three-isotope space. For the example of Mg, we assess appropriate quality control standards for interference–to-signal ratios and report apparent θ-values of carbonate-seawater pairs. We determined apparent θ–values for marine biogenic carbonates, where the foraminifera *Globorotalia menardii* yields 0.514 ± 0.005 (2 SD), the coral *Porites* 0.515 ± 0.006 (2 SD) and two specimens of the giant clam *Tridacna gigas* 0.508 ± 0.007 (2 SD) and 0.509 ± 0.006 (2 SD), documenting differences in the uptake pathway of Mg among marine calcifiers. The capability to measure apparent θ–values more precisely adds a new dimension to metal(loid) δ-values, with the potential to allow us to resolve different modes of fractionation in industrial and natural processes.

In most natural processes, stable isotopes are fractionated according to their relative mass difference or that of their isotopologues. In a few specific reactions, however, isotope abundances are shifted disproportionally to the relative mass differences of the isotopes or isotopologues. This effect is known as mass-independent isotope fractionation (MIF), and occurs for instance during chemical reactions in the gas phase of the sulfur cycle[1]. For elements with three or more stable isotopes such as O, Mg, Fe, Zn, and Mo the mass-dependence of isotope fractionation can be visualized by correlations in 'three-isotope plots', i.e. x-y scatter plots of two linearized δ-values. In this three-isotope space, mass-dependent isotope fractionation shifts materials along slopes that scale the two isotope ratios and that are known as the 'mass fractionation exponent' β[2] or 'triple isotope fractionation exponent' θ[3]. Fractionation laws predict minute but characteristic differences in the triple isotope fractionation exponents for equilibrium- and non-equilibrium mass-dependent stable isotope fractionation mechanisms[2]. Thus, the three-isotope relationship discloses information on the mechanism of isotope fractionation that cannot be obtained from δ-values. For instance, high-precision isotope ratio mass spectrometry (IRMS) measurements allow resolution of differences in oxygen's triple isotope composition[4,5], facilitating a range of applications including the quantification of O_2 production by global photosynthesis[6], the estimation of paleo-CO_2 concentrations from bioapatite[3], the distinction of diagenetic alteration in silicates and constraining paleo-hydrological conditions[7,8]. Recent progress in the theoretical and conceptual understanding of triple isotope fractionation[9,10] has advanced the field, especially for applications of O and S isotope analysis by IRMS. The current state-of-the-art in metal(loid) isotope ratio analysis, however, limits the resolution of the small isotopic differences stemming from differences in triple isotope fractionation exponents. Indeed, within the metal isotope community for most elements it is often considered sufficient to analyze one isotope ratio and infer the others assuming scaling factors[11]. The ability to analytically resolve the triple isotope exponent in metal(loid)s could, however, as in the case of O and S, open up a whole range of potential discoveries.

Current multicollector inductively-coupled plasma mass spectrometry (MC-ICPMS) approaches can permit typical precisions of ≈ 0.03 ‰ (2 SD) for metal(loid) isotope ratios. Such precision allows differences in three-isotope space to be resolved[12] provided the isotopic range exceeds 3 ‰ per amu[2]. Generally speaking, the measurement precision of θ increases with increasing isotopic range, because of the decreasing proportion of relatively invariant measurement uncertainty relative to the isotopic range. Thus to date, precise three-isotope compositions of metal isotopes have only been determined for data sets with large isotopic ranges, for instance those resulting from evaporation at high temperature (> 1600 °C), such as $\delta^{49/47}$Ti (19 ‰ range[13]), $\delta^{44/40}$Ca (99 ‰ range[13]), and $\delta^{26/24}$Mg (140 ‰[14]). At Earth surface conditions, the magnitude of stable metal isotope fractionation is much smaller, however, and so the limits of analytical precision often preclude the determination of θ-values. Mg

incorporation into calcite is associated with a relatively large magnitude of isotope fractionation, with $\alpha^{26/24}Mg_{calcite/solution}$ ranging from 0.9968 to 0.9981, i.e. 1000 ln α= 3.2 ‰ to 1.9 ‰[2,15–17]. Leveraging this large fractionation, a few studies have used three-isotope relationships in Mg to discuss isotope fractionation mechanisms in carbonate [12,17–19]. However, the vast majority of MC-ICP-MS-based studies employ the three-isotope relationship merely as a quality control indicator, i.e. sets of samples and standards must fall within the range of theoretically predicted θ-values of Young *et al.*[2] to be considered analytically robust. For instance, $\delta^{30/28}Si$ values that are too high in relation to corresponding $\delta^{29/28}Si$ values (assuming a 'normal' θ-value) can indicate $^{14}N^{16}O$ interference on ^{30}Si [20]. Even for this purpose, however, the impact of interferences has not been quantitatively assessed, and thus this approach can only be viewed as qualitative. Thus, despite recent advances in theoretical and conceptual work on triple isotope systematics[9,10], the potential of triple-isotope fractionation exponent measurements by MC-ICP-MS has yet to be fully exploited.

In this contribution, using Mg as an example, we explore the analytical limits of determining apparent triple isotope fractionation exponents (θ_{app}) of metal(loid) stable isotopes by MC-ICP-MS, and calculate an uncertainty budget for measured θ_{app}-values. We present a new measurement approach that significantly reduces analytical uncertainty, and determine quality control criteria for measurement of the three-isotope composition to warrant trueness and to maximize precision. As an example we determined the triple isotope fractionation exponent for Mg exchange on cation resin experimentally, and measured Mg θ_{app}-values in a range of marine biogenic carbonates, thereby demonstrating the precision achievable with our new measurement approach.

THEORY

Terminology

The notation of stable isotope ratios, including triple isotope systematics, have been comprehensively reviewed elsewhere[21–23]. As such, here we avoid replication and adopt the nomenclature suggested for the example of oxygen isotope ratios by Bao *et al.*[23], and refer the reader to this publication and the SI for more details. However, to provide a basis for subsequent discussion of uncertainty, we briefly summarize key points here. In a chemical reaction, stable isotopes are fractionated when they are transferred disproportionally between educt (*B*) and product (*A*). This change of isotope ratios between A and B is described by the isotope fractionation factor α. For elements with three or more stable isotopes (isotopes x, y, and z, where x < y < z), mass-dependent isotope fractionation yields correlated isotope ratios of intermediate-mass isotopes over the low-mass isotope, 'y/x' (*e.g.* $^{25}Mg/^{24}Mg$) and the high-mass isotope over the low-mass isotope, 'z/x' (*e.g.* $^{26}Mg/^{24}Mg$) for educts and products of a reaction (pathway). The isotope fractionation factors of the isotope ratios 'y/x' and 'z/x' in a given reaction are scaled by the 'triple isotope fractionation exponent' θ [3] (equation 1). θ is a property intrinsic to mass-dependent isotope fractionation, and will differ for equilibrium and non-equilibrium reactions.

$$\alpha^{y/x}_{A-B} = \alpha^{z/x}_{A-B}{}^{\theta} \qquad (1)$$

In practice, single reaction steps are difficult to isolate in multistage reaction pathways, and thus experimental and natural samples often integrate over a range of complex processes. In these cases the slope must be termed an "apparent θ-value", θ_{app}[9]. Measured θ_{app}-values of samples with a history of reactions and transport, and often also a spatial component (e.g. geological samples) are difficult to relate to intrinsic fractionation mechanisms at the molecular level. If such mechanisms can be ascertained to be conserved on the sample scale, however, θ_{app}-values can also be considered process-specific "diagnostic θ-values"[24]. Apparent θ-values can be obtained from the difference quotient of absolute isotope ratios of an element *E* in related samples *A* and *B*, or from their isotopic differences in δ-notation, provided they are first linearized as δ'-values[25] (equations 2, 3), an important prerequisite which has at times been overlooked.

$$\delta' E^{y,z/x}_{std} = \ln\left(\delta^{y,z/x}E_{std} + 1\right) \qquad (2)$$

$$\theta_{A-B} = \frac{\left(\delta'^{y/x}E(A)_{std} - \delta'^{y/x}E(B)_{std}\right)}{\left(\delta'^{z/x}E(A)_{std} - \delta'^{z/x}E(B)_{std}\right)} \qquad (3)$$

Crucially, for fractionation mechanisms to be deduced from regression lines fitted through linearized δ-values of sample sets, all samples must have been fractionated by the same mechanism, and must have had the same starting composition or a composition along the fractionation trend. In most geological and biological data sets, however, these requirements are not fulfilled, and therefore the slope contains no information on the fractionation mechanism and must be termed *S* [23].

A useful descriptive term for the three-isotope composition of single samples is the isotopic difference $\Delta'^{y/x}E$ between the samples' linearized δ-values and a reference line, *i.e.* a straight line slope in the linearized three-isotope space[8] (equation 4),

$$\Delta'^{y/x}E = \delta'^{y/x}E - \lambda \cdot \delta'^{z/x}E + \gamma \qquad (4)$$

where λ is the slope, and γ the y-intercept of the reference line. While the denominator x in the superscript is rarely used, it is necessary for elements with four or more isotopes for unambiguity. In principle any reference line can be used, but Δ'-values are comparable only when referenced to a common line. In metal(loid) stable isotope analysis by MC-ICP-MS, Δ'-values, when reported, are commonly referenced to theoretical slopes that represent specific end-members of mass-dependent isotope fractionation calculated from eqns. 15 (high-temperature equilibrium end-member; hereafter θ_{eq}) and 21 (non-equilibrium, atomic isotope fractionation end-member; hereafter θ_{non-eq_atomic}) in Young *et al.*[2] passing through the origin of the bracketing standard, typically the conventional δ-zero standard (in the case of Mg, DSM3[26]). Importantly, Δ'-values obtained from samples analyzed against different bracketing standards are comparable only when accounting for their difference in γ. The different ways of reporting the three-isotope relation are summarized in Fig. 1.

The uncertainty on apparent θ-values

The apparent triple isotope fractionation exponent can be deduced either from a sample-pair of educt and product of a chemical reaction or from sets of samples that stem from the same fractionation process. We evaluate the analytical limits
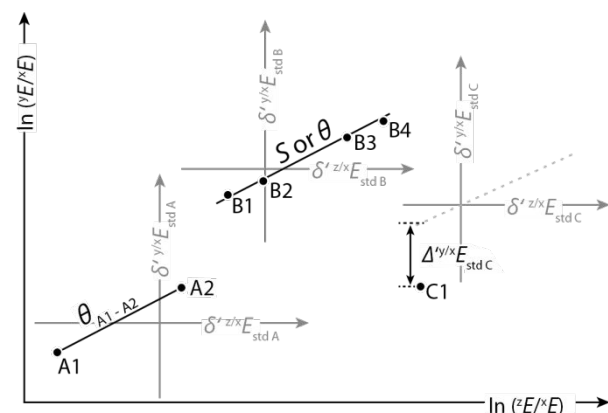
and measurement uncertainties of θ_{app}-values for sample pairs and sample sets.

Figure 1. The notation of different three-isotope relations schematically shown in linearized three-isotope space. Mass-dependent isotope fractionation shifts isotope ratios of samples along slopes θ, described by isotope fractionation laws. (Apparent) θ-values must be exclusively used when referring to sample pairs from one reaction (A1, A2) or sets of samples (B1 to B4) where all must derive from the same process. When a set of samples (B1 to B4) includes potentially unrelated samples, the slope must be referred to as S. $\Delta'^{y/x}E$ denotes the isotopic difference between a sample (C1) and a reference line.

To evaluate the uncertainty on apparent θ-values for sample pairs, we first calculated the uncertainty budget for $\delta^{25/24}Mg$ and $\delta^{26/24}Mg$ based on previous approaches[27,28]. This budget includes contributions from the isotope ratio measurements (R), sample digestion (κ_1) and ion chromatographic separation including the procedure blank (κ_2), the mass spectrometric background of the acid blank (κ_3), standard inhomogeneity (κ_4), instrumental mass bias drift (κ_5), matrix-dependent mass bias shift (κ_6) and residual interferences (κ_7) (values used are reported in Supporting Information 1). The uncertainty on $\delta'^{25,26/24}Mg$ is then calculated based on equation 5 below, where all κ_i have the value of unity and the associated uncertainty as described above.

$$\delta_{std}^{'y, z/24}Mg = \left(\frac{(R_{smp} \cdot \kappa_1 \cdot \kappa_2 \cdot \kappa_3 \cdot \kappa_6 \cdot \kappa_7)}{(R_{std} \cdot \kappa_4)} \cdot \kappa_5 \right) - 1 \quad (5)$$

The uncertainty u (standard uncertainty; $k= 1$; ≈ 68 % confidence level) can be calculated by using the partial derivatives of eqn. 5, by applying specific software such as GUM Workbench or by using the 'square sum approach' as shown in equation 6 below.

$$u(\delta_{std}^{'(y,z)/24}Mg) = \delta_{std}^{'(y,z)/24}Mg \sqrt{\left(\frac{u(R_{spl})}{R_{spl}}\right)^2 + \left(\frac{u(R_{std})}{R_{std}}\right)^2 + \sum_{i=1}^{7}\left(\frac{u(\kappa_i)}{\kappa_i}\right)^2} \quad (6)$$

This calculation yields an expanded uncertainty U (coverage factor; $k= 2$; ≈ 95 % confidence level) on $\delta^{25/24}Mg$ and $\delta^{26/24}Mg$ of 0.052 ‰ and 0.066 ‰, respectively, which is of the same order as the empirical 2 SD reproducibility of various rock standards (c.f. Teng, 2017). We detail the contributions to the uncertainty budget on δ-values in Supporting Information 1. The largest contribution to the uncertainty budget, and thus limitation on the uncertainty of δ-values, are sample digestion and preparation (up to 36 %) and the acid blank (up to 30 %).

As the θ_{app}-value of a sample pair is defined by the difference quotient of their linearized δ-values, it comprises uncertainty contributions from two $\delta'^{25/24}Mg$-values and two $\delta'^{26/24}Mg$-values, which are pairwise correlated. The uncertainty on θ can be obtained by performing a differentiation of eqn. 5 and including the covariances of the partial derivatives (Supporting Information 2). Calculated expanded uncertainties on θ are 0.031 (for $\Delta^{26/24}Mg_{A-B}= 1$ ‰), 0.017 (for $\Delta^{26/24}Mg_{A-B}= 2$ ‰), and 0.011 (for $\Delta^{26/24}Mg_{A-B}= 3$ ‰) (Fig. 2).

Reducing the uncertainty on apparent θ-values by sample-sample bracketing

To reduce the measurement uncertainty on apparent θ-values of sample pairs, we suggest a new and simple approach of direct bracketing of educt-product pairs that we refer to as *sample-sample-bracketing*. Typically, to compensate for the problem of drifting mass bias in MC-ICPMS analysis, standards and samples must be measured alternately via a procedure known as standard-sample-bracketing. Whilst effective in obtaining accurate data, this introduces additional uncertainties associated with the measurements of the standard (R_{std}, see equation 5).

When sample-pairs are instead alternately measured, rather than each against their own bracketing standards, the uncertainty on (apparent) θ will be reduced, because then only two δ-value measurements contribute to the uncertainty budget of the (apparent) θ-value (Supporting Information 2). By this approach the calculated uncertainties on θ ($k= 2$) are reduced to 0.022 (for $\Delta^{26/24}Mg_{A-B}= 1$ ‰), 0.012 (for $\Delta^{26/24}Mg_{A-B}= 2$ ‰), and 0.008 (for $\Delta^{26/24}Mg_{A-B}= 3$ ‰); ≈ 30 % lower than on θ-values derived via standard-sample-bracketing. Fig. 2 shows uncertainties for θ-values calculated via this approach in comparison to standard-sample bracketing, as a function of isotopic difference $\Delta^{26/24}Mg_{A-B}$.

To validate these calculations empirically, we determined the standard deviation on measured θ_{app}-values of sample-pairs. We also demonstrate the phenomenon of increasing precision with increasing isotopic difference for a range of published Mg and Si data sets (Supporting Information 3, Supporting Fig. S1). The reproducibility on θ_{app}-values (2 SD) should be better than the estimated uncertainty ($k= 2$), however, trueness of (apparent) θ might not be warranted at the 2 SD reproducibility. We suggest using our calculated uncertainty on (apparent) θ when the analytical conditions are comparable to those reported here and provided that the 2 SD reproducibilities are $\leq$ the expanded uncertainty; $k= 2$. Our uncertainty assessment suggests that a difference in the θ-value of 0.01 (i.e. the range of values for the end-member cases θ_{eq} and θ_{non-eq_atomic} [2]) can be resolved at the ≈ 68 % confidence level when the isotopic difference of the sample pairs is ≥ 2 ‰ $\Delta^{26/24}Mg_{A-B}$ and on the ≈ 95 % confidence level when the isotopic difference of the sample pairs is ≥ 4 ‰. For lower magnitudes of isotope fractionation the uncertainty on (apparent) θ-values is too large to confidently resolve differences in triple isotope fractionation exponents.
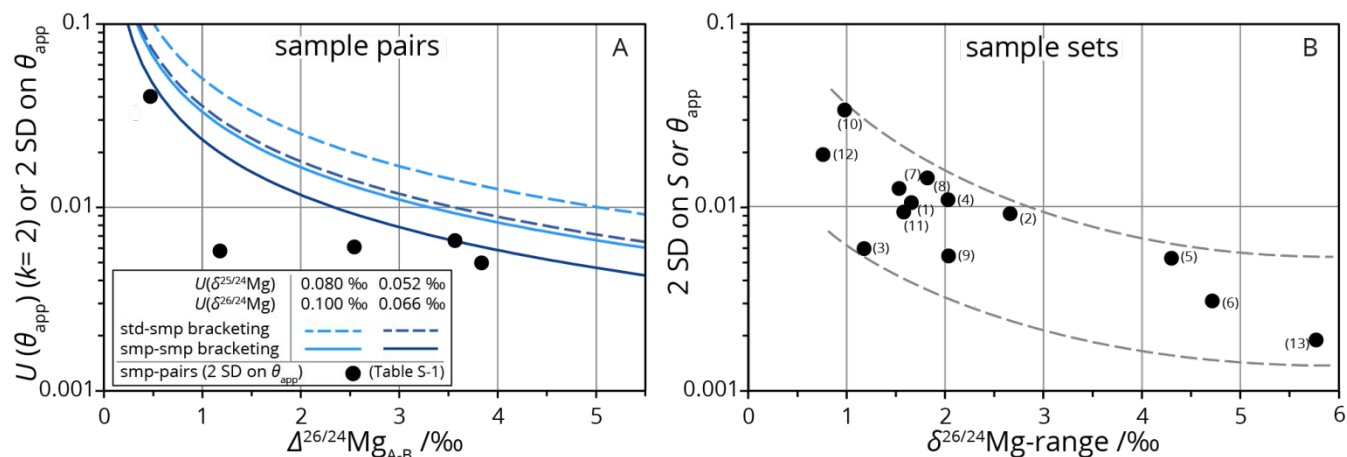
Figure 2. Uncertainty and standard deviations on apparent θ-values of sample pairs and standard deviations on slopes in sample sets. A) calculated expanded uncertainty (curves; k= 2; Supporting information 1), and empirically determined 2 SD on the slope between sample pairs (points; Supporting Table S1). B) Two standard deviations on the slope of regression lines extracted from published data sets 1[29], 2[18], 3[30], 4[31], 5[32], 6[15], 7[33], 8[34], 9[35], 10[36], 11[37], 12[38], 13: this study.

1 For elements with more than three stable isotopes, (apparent) θ–values can be determined for different combinations of isotopes. Provided that the isotope ratios can be measured precisely, isotopes can be selected to maximize the mass difference and thus the isotopic difference $\Delta'^{25/24}Mg$ for given triple isotope fractionation exponents, which yields an increased resolution of θ_{app}–values. As an example, the range of θ-values for Mo can be expanded (by $\approx$ 32 % for the end-member cases in Young *et al.*[2]) when the isotopes 92, 96 and 100 are used instead of 92, 95 and 98 (Supporting Fig. S2).

For sets of samples that stem from the same fractionation process, the overall uncertainty on (apparent) θ-values depends on the uncertainty of each individual δ-value, the range of δ-values and their distribution within that range. Therefore, the uncertainty on (apparent) θ- or S-values of sample sets cannot be generalized. However, if analytical conditions are comparable to those reported above, we suggest that for simplicity the uncertainty can be approximated by the standard deviation on the slope of the regression line fitted through the δ'-values. The uncertainty on the slope can be assessed precisely when the standard deviation of every δ-value is accounted for. To determine the standard deviation on the slope of a data set of Mg fractionated on cation resin (see discussion), we used the software GUM workbench (by Metrodata) that performs uncertainty calculations based on a numerical differentiation and a Monte-Carlo simulation of the provided equations. The standard deviation on the slope of regression lines can also be approximated by a least square calculation where only the mean values of the samples are considered.

To determine typical standard deviations on apparent θ- or S-values for sample sets, we evaluated a range of published data sets using least square calculations. These sample sets of speleothems[15,18], foraminifera[39], plants[29,38], bioapatite[33,34], carbonates[30,31,35] and fungi[37] yield standard deviations in the range of 0.003 to 0.034, generally decreasing with increasing isotopic variation (Fig. 2 B). Variations in standard deviations for given isotopic differences might result not only from variable data quality, but also from differences in fractionation histories within the data sets.

Avoiding biases on apparent θ-values

To obtain true (apparent) θ-values, elements that cause interferences on one or more analyte metal(loid) isotope must be thoroughly chemically separated, or the interferences must be resolved mass-spectrometrically. Although minor interferences may not impact the trueness of δ-values within quoted analytical precision, they can bias θ-values, even if they are invisible in high resolution mass spectra. In the case of Mg, numerous interferences in the mass range of the isotopes of Mg have the potential to bias apparent θ-values. Interferences of doubly charged Ti and Cr can be important for silicates, but they are rarely an issue in carbonates because these elements are typically of very low concentrations in carbonates. Mg hydrides were shown to be insignificant even under wet plasma conditions[40]. C- and N-based interferences can be resolved by using the medium mass resolution mode (resolving power $\approx$ 5000) and performing measurements on the low- mass side of the Mg peak, however, the $^{48}Ca^{++}$ interference cannot be resolved at the same time (Supporting Fig. S3). Since many geological, environmental and biological samples contain Ca- and C-rich matrices, this can be problematic.

In Ca-rich samples, such as most carbonates or calcium phosphates, a single ion chromatographic separation step can be insufficient to fully remove Ca. We evaluate the impact of residual $^{48}Ca^{++}$ interference on the trueness of θ-values over a typical range in Mg-Ca ratios of between 1 and 50. The interference-to-analyte ratio $^{48}Ca^{++}/^{24}Mg$ remains relatively low despite relatively high Ca concentrations, due to the low isotopic abundance of ^{48}Ca (0.187 %) and the low formation rate of doubly charged Ca ions of ca. 0.1 % (as determined by sector field ICP-MS). However, although seemingly low, interference-to-analyte ratios of > 10^{-6} have a significant impact on θ_{app} (Fig. 3). For instance, for a sample pair with 500 ng g^{-1} Mg that differ by 1.5 ‰ $\delta^{26/24}Mg$, increasing Ca concentrations from 0 ng g^{-1} to 50 ng g^{-1} (*i.e.* $\Delta Ca/Mg$ = 0.1) will bias the θ_{app} -value by $\approx$ 0.001. Thus, for the measurement of θ_{app}, the Ca/Mg difference between samples A and B should be low enough that the bias in θ_{app} is kept below 0.001. As the bias depends on the isotopic difference between samples A and B, the tolerance level of Ca/Mg will change accordingly. The impact of interferences on Δ'-values is equivalent to that

described for θ_{app}-values (Supporting Fig. S4). We note however that δ-values are much less affected by the $^{48++}$Ca interference. Ca/Mg differences as high as 0.2 only yield an interference-related shift in $\delta^{26/24}$Mg of ≈ 0.006 ‰, which is low compared to the natural range of $\delta^{26/24}$Mg-values. This assessment does not account for matrix-related bias of measured isotope ratios.

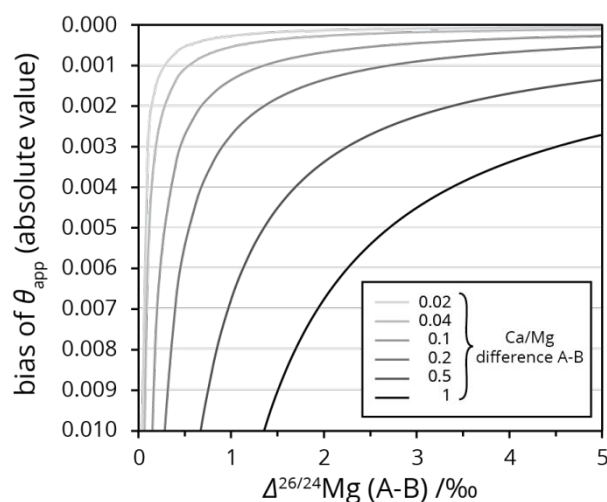**Figure 3.** Bias of θ_{app} of sample pairs with isotopic differences ≤ 5 ‰ and Ca/Mg between 0.02 and 1. The sign of bias depends on whether sample A or B has the higher Ca/Mg.

RANGES OF θ-VALUES

Theoretical ranges of triple isotope fractionation exponents can be predicted from the quantum mechanical behavior of isotopes and their kinetic energy[2]. The commonly assumed range of θ-values of Mg is 0.521 to 0.511, when using atomic masses in eqns. 15 (θ_{eq}) and 21 (θ_{non-eq_atomic}) in Young et al.[2]. However, these equations represent specific end-member cases and are not representative of the full range of apparent θ-values that can be observed in nature. We take this opportunity to highlight how transport of isotopologues and simple multi-step fractionation can expand this range of apparent θ-values.

θ_{eq}[2] is a special end-member value for bonds or molecules at high-temperature and has a fixed value of 0.521 for Mg. As this value is predominantly controlled by isotope mass, it is largely temperature-independent[2,41]. However, other equilibria, e.g. between reactant and transition state (termed kinetic isotope effects) and non-equilibrium processes (isotope substitution reactions where the isotope fractionation effect is determined by the ratio of the rate-constants[42]) can produce varying values of θ. In bond-breaking reactions, e.g. the dehydration of Mg isotopologues, reduced masses (the effective mass of two interacting bodies, m1* m2/(m1+m2)) might be relevant[2]. Thus, isotope fractionation during bond-breaking is expected to yield θ-values larger than those based on atomic masses ($\theta_{non-eq\_atomic}= 0.511$; eqn. 21 in Young et al.[2]). For instance, θ-values can be as high as 0.517 for Mg + 1 water molecule. In comparison, during transport, effective molecular masses in motion control non-equilibrium effects[2]. θ-values will decrease with increasing isotopologue mass and approach a value that is lower than 0.511 by the ratio of the mass differences (^yE - ^xE)/(^zE - ^xE). For Mg this difference amounts 0.010 and thus isotopologue fractionation during transport approaches $\theta= 0.501$ (Supporting Fig. S2). Notably,

with increasing molecular mass the relative mass difference between the isotopologues decreases and with it the magnitude of isotope fractionation, making precise θ-value measurements difficult.

Observed θ-values can also be beyond this range when sample pairs are mistaken to represent one single fractionation step, when in reality they represent a pathway comprising two or more subsequent reactions[9]. When the sign of isotope fractionation is identical, such 'composite' apparent θ-values will attain values within these bounds. However, apparent θ-values outside this range can result when the fractionation sequence comprises both different fractionation mechanisms and different directions of isotope fractionation. Depending on the magnitudes of isotope fractionation, an apparent θ-value can be < 0.501 or > 0.521. An example for an apparent 'composite' θ-value > 0.521 is a sublimation-condensation reaction as represented by ERM-AE145 that was produced by high vacuum sublimation and condensation of ERM-AE144[40]. The apparent θ-value is ~ 0.6 and most likely results from non-equilibrium fractionation during sublimation that enriched the gas phase in the low-mass Mg isotopes, followed by equilibrium isotope fractionation during condensation that enriched the solid in the high-mass Mg isotopes. For these types of sequential fractionation processes, the overall apparent θ-value is weighted for each individual fractionation step (equation 6 in Hayles et al.[10]). For further examples of how complex reservoir and transport effects and multiple reaction steps can result in extreme θ_{app}-values, we refer the reader to Bao et al.[9].

MATERIALS AND METHODS

To demonstrate the benefits of our sample-sample bracketing approach, we determined apparent θ-values for Mg in marine biogenic carbonates and one biogenic phosphate sample.

Specifically, we analyzed a set of samples of modern marine biogenic carbonates including JCp-1 (Geological Survey of Japan, *Porites*, coral[43]), JCt-1 (Geological Survey of Japan, *Tridacna gigas*, clam shell), EN-1 (U.S. Geological Survey, *Tridacna gigas*, clam shell), and a sample of the foraminifera *Globorotalia menardii* from Holocene core-top sediment from the Gulf of Aden. We also analyzed dentin from a modern great white shark (*Carcharadon carcharias*) from off the coast of South Africa (sample GW-1 from Vennemann et al.[44]) and modern seawater (NRC Canada, North Atlantic seawater; NASS-6). Moreover, we analyzed the reference materials JDo-1, BHVO-2, and JLs-1 (Supporting Table S2) and a series of SI-traceable Mg isotope reference materials including ERM-AE143, ERM-AE144, ERM-AE145 [40] and the δ–zero standard DSM3[26]. In addition, we deliberately fractionated Mg dissolved in acidic aqueous solution on cation exchange resin, to determine θ for Mg in an equilibrium exchange reaction.

With the exception of foraminiferal carbonates, bulk, ground bioapatite and carbonate powder aliquots of 1 - 18 mg were digested at 150°C in concentrated, double-distilled HNO_3 or in HNO_3-H_2O_2 mixtures using an acid sample digestion system (DAS from PicoTrace®). In the case of foraminifera, we followed different protocols to avoid the inclusion of contaminant clay, which may be rich in Mg that is of very different isotope composition [45].

Following evaporation, all samples were redissolved in 2 mL HNO_3 (1 mol L^{-1}) for chromatographic ion separation using $\approx$ 2.6 mL of AG 50W-X12 cation exchange resin in

polypropylene columns (Kimble™ Kontes™ Disposaflex), where Mg was eluted with 10 mL M HNO_3 (2 mol L^{-1}). A second purification step was performed for samples with residual calcium > 50 ng g^{-1}. The dried Mg-fraction was re-dissolved in concentrated HNO_3 to remove organic matter derived from the cation exchange resin. External standards and Mg reference materials yielded δ-values in agreement with published values (Supporting Tables S2, S3). Mg recovery rates were quantitative within analytical uncertainty. Splits of the fractions before and after the Mg elution peak were screened for Mg, to monitor successful separation of Mg from other cations. To ensure that the Mg peak did not shift due to varying matrix composition, we determined the relative mass fraction of Mg in these splits relative to that in the splits plus the Mg-fraction, with these values always being below 0.1 %. Procedural blanks were always < 7 ng Mg, of which < 2 ng derived from the column procedure. All standards and samples were diluted in HNO_3 (0.32 mol L^{-1}) for Mg isotope ratio measurements by MC-ICP-MS in medium resolution mode (Neptune Plus at BAM in Berlin and at GFZ Potsdam) using a normal nickel sample and a X skimmer cone. Samples and standards were measured at concentrations between 0.5 and 1 ppm Mg, where samples and bracketing standard concentrations were matched to < 15 %. We used a stable introduction system (SIS) quartz glass spray chamber equipped with a self-aspirating micro-concentric PFA nebulizer with an effective uptake rate of 165 µL min^{-1}.

We used two different approaches to determine θ_{app}–values. To determine the triple isotope fractionation exponent from a sample set (Mg fractionated on a cation exchange resin) we used conventional standard-sample-bracketing and a regression analysis. To determine θ_{app}-values for carbonate- or apatite- seawater pairs, we used our new sample-sample bracketing approach

RESULTS AND DISCUSSION

Mg triple isotope fractionation during Mg uptake from seawater into carbonate

Different mechanisms of carbonate formation are likely characterized by distinct and specific triple isotope fractionation exponents, as there may be different underlying physicochemical processes (e.g. diffusion, coordination, equilibrium partitioning, surface properties, and variable bond strength). Thus, the characterization of apparent θ-values for Mg uptake into biogenic carbonates might allow modes of Mg

uptake to be constrained. Seawater Mg isotope composition is homogenous[46], and as such NASS-6 (NRC Canada) can be assumed to be representative of the educt for the precipitation of all marine biominerals, and thus used for sample-sample bracketing.

While previous work suggests predominantly non-equilibrium isotope fractionation for marine calcifiers[19], we can resolve for the first time differences in the apparent triple isotope fractionation exponents that attest to differences in the mechanisms of Mg uptake. θ_{app} for the Mg uptake from seawater into the low-Mg calcite planktic foraminifera *Globorotalia menardii* was determined as $\theta_{app}= 0.514 \pm 0.005$ (2 SD), identical to that of the aragonitic coral *Porites* (JCp-1) at $\theta_{app}= 0.514 \pm 0.006$ (2 SD). The two specimens of the giant clam *Tridacna gigas* (EN-1 and JCt-1) yielded identical θ_{app}-values of 0.508 ± 0.007 (2 SD) and 0.509 ± 0.006 (2 SD), respectively. The apparent θ-value between seawater and dentin bioapatite of a shark tooth of *Carcharodon carcharias* (sample DHai6) was measured as 0.511 ± 0.040 (2 SD) (Fig. 4). This value is too imprecise to distinguish isotope fractionation pathways due to the too low isotopic difference between the tooth dentin and seawater of 0.48 ‰ $\delta^{26/24}Mg$ (cf. Fig. 2).

The giant clam *Tridacna gigas* (JCt-1 and EN-1) yields apparent θ-values identical within uncertainty to the theoretical θ_{non-eq_atomic}. The values also agree with fractionation of isotopologues of Mg during transport; an isotopic fingerprint preserved through the entrapment of hydrated Mg during high rates of precipitation[17]. The foraminifera *Globorotalia menardii* and the coral *Porites* yield apparent θ-values between θ_{eq} and θ_{non-eq_atomic}. This could either suggest non-equilibrium dissociation where reduced masses apply[2] or multi-stage isotope fractionation with different fractionation mechanisms involved. When published Mg isotope data from foraminifera[45] are evaluated using our seawater δ-values of -0.43 ‰ $\delta^{25/24}Mg$ and -0.83 ‰ $\delta^{26/24}Mg$, θ_{app} –values are identical to θ_{eq} in the species *Globorotalia tumida*, *Globigerinoides ruber* and *Globigerinoides sacculifer* that yield 0.524 ± 0.007 (2 SD, n= 3), 0.522 ± 0.013 (2 SD, n= 4) and 0.521 ± 0.012 (2 SD, n= 3), respectively. Hippler *et al.*[32] report a data set including red algae, echinoids, brachiopods, *Mytilus edulis*, one scaphopod, seawater and DSM3 that fall onto a slope identical to θ_{eq} with S= 0.521 ± 0.004. However, as discussed earlier, such S-values involving unrelated samples cannot
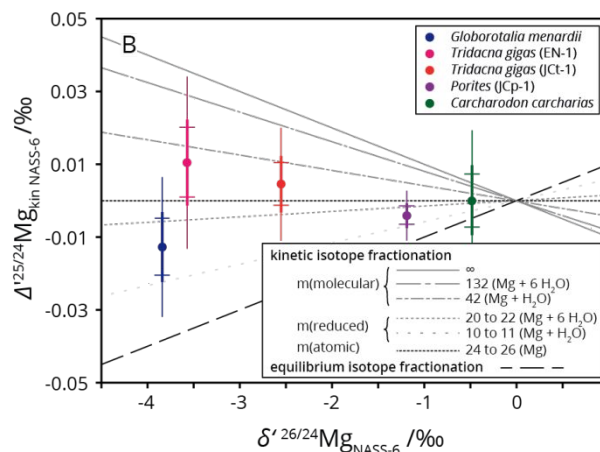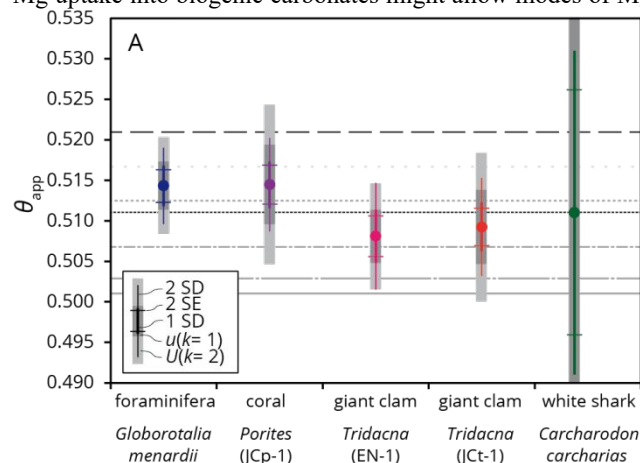
Figure 4. θ-values (A) and Δ'-values vs δ'-values (B) of biogenic carbonates and bioapatite obtained by sample-sample bracketing against seawater (NASS-6). The slopes plotted represent special cases of non-equilibrium processes based on atomic mass, molecular and reduced masses corresponding to Mg with one and six water molecules (the inner hydration sphere) as well as equilibrium isotope fractionation.

inform as to fractionation mechanisms. If θ_{app}-values are instead calculated by pairing individual species with their seawater educts, and assuming comparable analytical conditions as in this study, θ-values deviate from this value: the red algae yield 0.515 ± 0.005 (2 SD, n= 6), the echinoids 0.512 ± 0.010 (2 SD, n= 7), the brachiopods 0.513 ± 0.013 (2 SD, n= 2), the *Mytilus edulis* 0.512 ± 0.013 (2 SD, n= 15) and the scaphopod 0.533 (n= 1). To obtain a clearer picture of the variability of triple isotope fractionation exponents in biogenic carbonates, we suggest systematic studies using the sample-sample bracketing approach against seawater are required.

At this stage, it is unclear whether the Mg isotope fractionation in marine calcifiers arises at the growing crystal face[47], or whether fractionation is induced during some earlier manipulation of the calcifying fluid. For instance, low-Mg calcite foraminifera (such as those measured here) are thought to remove Mg from a calcification pool of vacuolized seawater to promote calcification[48], either through pumping[49], or precipitation and subsequent isolation of high-Mg phases[50]. Alternatively, low-Mg calcite planktonic foraminifera might synthesize biomolecules that increase the energy barrier for Mg incorporation[19]. Further investigation of Mg θ_{app}-values in high-Mg calcite benthic foraminifera such as *Operculina ammonoides* that precipitates its shell from seawater without removal of Mg from its calcifying fluid[51], may help to inform as to the cause of Mg isotope fractionation. It is also intriguing to note that our two measurements of *Tridacna* are identical and show a lower θ_{app}-value compared to *G. menardii* and *Porites* coral. This could reflect tighter biological mediation (and hence potentially multiple superimposed fractionation processes) during calcification in moluscans[52] compared to foraminifera and corals, where directly-vacuolized seawater is involved in calcification[48]. That said, we acknowledge that even with our new approach this is only resolvable at the 1 SD level; higher analytical precision and/or more measurements on the same species are needed to verify this at 95% confidence.

Mg triple isotope fractionation on cation resin

Cations can be separated from a sample matrix by cation exchange resins, such as AG W50-X12 that consists of a styrene divinylbenzene copolymer lattice with attached sulfonic acid functional groups. Upon sample loading, counterions (H^+) on the resin are replaced by ions from the sample, which can then be eluted from the resins by exchanging them with H^+ ions using acids. The partitioning of cations between solution and the resin can be assumed to be in equilibrium[51]. As the binding energy differs among the isotopes of an element, isotopes are fractionated during the exchange between solution and resin. Given this equilibrium partitioning of stable isotopes, it seems plausible that isotope fractionation follows the equilibrium mass-dependent fractionation law. To determine the type of fractionation mechanism by measurement, we loaded 39 µg Mg from a Mg-solution produced from pure metal turnings (purity ≥0.999 g g^{-1}) onto a cation exchange column and analyzed four separate splits of the elution volume of Mg as well as the original solution. The splits were measured against an in-house standard (isotopically enriched for test purposes) and re-

calculated to the DSM3 scale (Supporting Table S4) using Supporting equation S9. Regression analysis on δ'-values yields a slope 0.520 ± 0.002 (2 SD), where the standard deviation is determined from average δ'-values (Fig. 5). The expanded uncertainty of the regression line is 0.0034 (k= 2) when determined based on the individual analytical standard
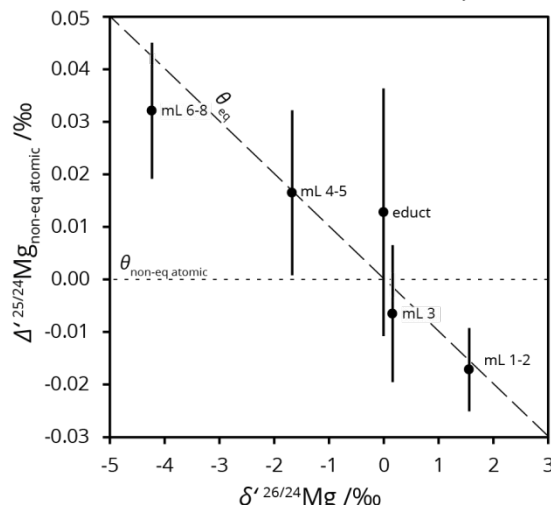

Figure 5. Mg isotope fractionation on AG W50-X12 cation exchange resin. Three-isotope plot Δ' vs. δ'-value plot (δ'-values recalculated versus the educt solution before ion separation). Error bars represent 1 SD from replicate measurements.

deviations of each sample (using GUM workbench). Interestingly, this slope is identical to θ_{eq}. This example demonstrates that differences in fractionation mechanism can be resolved analytically on the 95% confidence level for sets of samples (from one fractionation process) when the isotopic range is large (here 5.79 ‰ $\Delta^{26/24}$Mg). We also evaluated previously published Mg isotope data that documents fractionation on AG50W-X8 resin during a HCl-based two-step chromatographic Mg separation[55]. Interestingly, these data fall onto a distinct slope of 0.500 ± 0.002 (2 SD) conforming to non-equilibrium high-mass fractionation during transport of isotopologues. Isotopologues of $MgCl_2$ are predicted to fractionate along a slope of 0.5036, close to the observed value, suggesting that fractionation occurs during transport of this molecule.

CONCLUSIONS

Our new measurement approach of direct sample-sample bracketing allows the apparent triple-isotope fractionation exponent θ_{app} of metal(loid) stable isotopes to be determined with ≈ 30% lower uncertainty than previously possible. With these more precise measurements different modes of mass-dependent stable isotope fractionation can now be resolved by MC-ICP-MS at the 1 SD level where isotopic differences of educt-product pairs are ≥ 2 ‰ per 2 amu mass difference. The possibility to infer stable isotope fractionation reaction mechanisms directly by such measurements thus extends the utility of metal(loid) stable isotope ratios beyond the δ-scale. While future work is needed to calibrate diagnostic θ-values and test models of stable isotope fractionation mechanisms,

with this new approach a broad range of questions in the natural sciences can be addressed that have up to now been beyond our reach.

ASSOCIATED CONTENT

AUTHOR INFORMATION

Corresponding Author

* mtatzel@ucsc.edu

Present Addresses

† Institute of Marine Sciences, University of California Santa Cruz, 1156 High Street, Santa Cruz, CA 95064, USA

Author Contributions

The manuscript was written through contributions of all authors. All authors have approved the final version of the manuscript.

ACKNOWLEDGMENT

REFERENCES

(1) Farquhar, J.; Bao, H.; Thiemens. *Science* **2000**, *289* (5480), 756–759.
(2) Young, E. D.; Galy, A.; Nagahara, H. *Geochim. Cosmochim. Acta* **2002**, *66* (6), 1095–1104.
(3) Pack, A.; Gehler, A.; Süssenberger, A. *Geochim. Cosmochim. Acta* **2013**, *102*, 306–317.
(4) Pack, A.; Herwartz, D. *Earth Planet. Sci. Lett.* **2014**, *390*, 138–145.
(5) Sengupta, S.; Pack, A. *Chem. Geol.* **2018**, *495* (July), 18–26.
(6) Luz, B.; Barkan, E.; Bender, M.; Thiemens, M. H.; Boering, K. A. *Nature* **1999**, *400*, 547–550.
(7) Herwartz, D.; Pack, A.; Krylov, D.; Xiao, Y.; Muehlenbachs, K.; Sengupta, S.; Di Rocco, T. *Proc. Natl. Acad. Sci.* **2015**, *112* (17), 5337–5341.
(8) Sharp, Z. D.; Gibbons, J. A.; Maltsev, O.; Atudorei, V.; Pack, A.; Sengupta, S.; Shock, E. L.; Knauth, L. P. *Geochim. Cosmochim. Acta* **2016**, *186*, 105–119.
(9) Bao, H.; Cao, X.; Hayles, J. A. *Geochim. Cosmochim. Acta* **2015**, *170*, 39–50.
(10) Hayles, J. A.; Cao, X.; Bao, H. *Geochemical Perspect. Lett.* **2017**, 1–6.
(11) Wiederhold, J. G. *Environ. Sci. Technol.* **2015**, *49* (5), 2606–2624.
(12) Young, E. D.; Galy, A. *Rev. Mineral. Geochemistry* **2004**, *55* (1), 197–230.
(13) Zhang, J.; Huang, S.; Davis, A. M.; Dauphas, N.; Hashimoto, A.; Jacobsen, S. B. *Geochim. Cosmochim. Acta* **2014**, *140*, 365–380.
(14) Davis, A. M.; Richter, F. M.; Mendybaev, R. A.; Janney, P. E.; Wadhwa, M.; McKeegan, K. D. *Geochim. Cosmochim. Acta* **2015**, *158*, 245–261.
(15) Immenhauser, A.; Buhl, D.; Richter, D.; Niedermayr, A.; Riechelmann, D.; Dietzel, M.; Schulte, U. *Geochim. Cosmochim. Acta* **2010**, *74* (15), 4346–4364.
(16) Li, W.; Chakraborty, S.; Beard, B. L.; Romanek, C. S.; Johnson, C. M. *Earth Planet. Sci. Lett.* **2012**, *333–334*, 304–316.
(17) Mavromatis, V.; Gautier, Q.; Bosc, O.; Schott, J. *Geochim. Cosmochim. Acta* **2013**, *114*, 188–203.
(18) Buhl, D.; Immenhauser, A.; Smeulders, G.; Kabiri, L.; Richter, D. K. *Chem. Geol.* **2007**, *244*, 715–729.
(19) Wombacher, F.; Eisenhauer, A.; Böhm, F.; Gussone, N.; Regenberg, M.; Dullo, W. C.; Rüggeberg, A. *Geochim. Cosmochim. Acta* **2011**, *75* (19), 5797–5818.
(20) Fontorbe, G.; Frings, P. J.; De La Rocha, C. L.; Hendry, K. R.; Conley, D. J. *Earth Planet. Sci. Lett.* **2016**, *453*, 67–77.
(21) Ono, S.; Wing, B.; Johnston, D.; Farquhar, J.; Rumble, D. **2006**, *70*, 2238–2252.
(22) Eiler, J. M.; Bergquist, B. A.; Bourg, I. C.; Cartigny, P.; Farquhar, J.; Gagnon, A.; Guo, W.; Halevy, I.; Hofmann, A. E.; Larson, T. E.; Levin, N. E.; Schauble, E. A.; Stolper, D. *Chem. Geol.* **2014**, *372*, 119–143.
(23) Bao, H.; Cao, X.; Hayles, J. A. *Annu. Rev. Earth Planet. Sci.* **2016**, *44* (1), 463–492.
(24) He, Y.; Bao, H. *ACS Earth Sp. Chem.* **2019**, *3*, 120–128.
(25) Hulston, J. R.; Thode, H. G. *J. Geophys. Res.* **1965**, *70* (14), 3475–3484.
(26) Galy, A.; Yoffe, O.; Janney, P. E.; Williams, R. W.; Cloquet, C.; Alard, O.; Halicz, L.; Wadhwa, M.; Hutcheon, I. D.; Ramon, E.; Carignan, J. *J. Anal. At. Spectrom.* **2003**, *18* (11), 1352–1356.
(27) Rosner, M.; Pritzkow, W.; Vogl, J.; Voerkelius, S. *Anal. Chem.* **2011**, *83* (7), 2562–2568.
(28) Geilert, S.; Vogl, J.; Rosner, M.; Voerkelius, S.; Eichert, T. *Mass Spectrom. Purif. Tech.* **2015**, *1* (1), 1–6.
(29) Bolou-Bi, E. B.; Vigier, N.; Poszwa, A.; Boudot, J.-P. P.; Dambrine, E. *Geochim. Cosmochim. Acta* **2012**, *87*, 341–355.
(30) Geske, A.; Lokier, S.; Dietzel, M.; Richter, D. K.; Buhl, D.; Immenhauser, A. *Chem. Geol.* **2015**, *393–394*, 112–124.
(31) Geske, A.; Goldstein, R. H.; Mavromatis, V.; Richter, D. K.; Buhl, D.; Kluge, T.; John, C. M.; Immenhauser, A. *Geochim. Cosmochim. Acta* **2015**, *149*, 131–151.
(32) Hippler, D.; Buhl, D.; Witbaard, R.; Richter, D. K.; Immenhauser, A. *Geochim. Cosmochim. Acta* **2009**, *73* (20), 6134–6146.
(33) Martin, J. E.; Vance, D.; Balter, V. *Geochim. Cosmochim. Acta* **2014**, *130*, 12–20.
(34) Martin, J. E.; Vance, D.; Balter, V. *Proc. Natl. Acad. Sci.* **2015**, *112* (2), 430–435.
(35) Mavromatis, V.; Pearce, C. R.; Shirokova, L. S.; Bundeleva, I. A.; Pokrovsky, O. S.; Benezeth, P.; Oelkers, E. H. *Geochim. Cosmochim. Acta* **2012**, *76*, 161–174.
(36) Pogge von Strandmann, P. A. E.; Olsson, J.; Luu, T.; Gislason, R.; Burton, K. W.; Pearce, C. R. *Front. Earth Sci.* **2019**, *7* (February), 1–9.
(37) Pokharel, R.; Gerrits, R.; Schuessler, J. A.; Floor, G. H.; Gorbushina, A. A.; von Blanckenburg, F. *Environ. Sci. Technol.* **2017**, *51* (17), 9691–9699.
(38) Uhlig, D.; Schuessler, J. A.; Bouchez, J.; Dixon, J. L.; von Blanckenburg, F. *Biogeosciences* **2017**, *14* (January), 3111–3128.
(39) Pogge von Strandmann, P. A. E. *Geochemistry, Geophys. Geosystems* **2008**, *9* (12).
(40) Vogl, J.; Brand, B.; Noordmann, J.; Rienitz, O.; Malinovskiy, D. *J. Anal. At. Spectrom.* **2016**, *31*, 1440–1458.
(41) Dauphas, N.; Schauble, E. A. *Annu. Rev. Earth Planet. Sci.* **2016**, *44* (1), 709–783.
(42) Clayton, R. N.; Mayeda, T. K. *J. Phys. Chem. A* **2009**, *113* (10), 2212–2217.
(43) Okai, T.; Suzuki, A.; Kawahata, H.; Terashima, S.; Imai, N. *Geostand. Newsl.* **2002**, *26*, 95–99.

(44) Vennemann, T. W.; Hegner, E.; Cliff, G.; Benz, G. W. *Geochim. Cosmochim. Acta* **2001**, *65* (10), 1583–1599.

(45) Pogge von Strandmann, P. A. E.; Forshaw, J.; Schmidt, D. N. *Biogeosciences* **2014**, *11* (18), 5155–5168.

(46) Foster, G. L.; Pogge von Strandmann, P. A. E.; Rae, J. W. B. *Geochemistry, Geophys. Geosystems* **2010**, *11* (8), 1–10.

(47) DePaolo, D. J. *Geochim. Cosmochim. Acta* **2011**, *75* (4), 1039–1056.

(48) Bentov, S.; Brownlee, C.; Erez, J. *Proc. Natl. Acad. Sci.* **2009**, *106* (51), 21500–21504.

(49) Bentov, S.; Erez, J. *Geochemistry, Geophys. Geosystems* **2006**, *7* (1), 1–11.

(50) Khalifa, G. M.; Kirchenbuechler, D.; Koifman, N.; Kleinerman, O.; Talmon, Y.; Elbaum, M.; Addadi, L.; Weiner, S.; Erez, J. *J.* *Struct. Biol.* **2016**, *196* (2), 155–163.

(51) Evans, D.; Müller, W.; Erez, J. *Geochim. Cosmochim. Acta* **2018**, *236*, 198–217.

(52) Weiner, S.; Dove, P. M. *Rev. Mineral. Geochemistry* **2003**, *54* (1), 1–29.

(53) Glueckauf, E. *Trans. Faraday Soc.* **1955**, *51*, 34–44.

(54) Zhu, X. K.; Guo, Y.; Williams, R. J. P.; O'Nions, R. K.; Matthews, A.; Belshaw, N. S.; Canters, G. W.; Waal, E. C. De; Weser, U.; Burgess, B. K.; Salvato, B. *Earth Planet. Sci. Lett.* **2002**, *200*, 47–62.

(55) Chang, V. T.-C.; Makishima, A.; Belshaw, N. S.; O'Nions, R. K. *J. Anal. At. Spectrom.* **2003**, *18*, 296–301.

For Table of Contents Only